

# Data based reconstruction of complex cyberphysical networks

Chuang Ma,<sup>1</sup> Han-Shuang Chen,<sup>2</sup> Xiang Li,<sup>3</sup> Ying-Cheng Lai,<sup>4</sup> and Hai-Feng Zhang<sup>1,5,\*</sup>

<sup>1</sup>*School of Mathematical Science, Anhui University, Hefei 230601, China*

<sup>2</sup>*School of Physics and Material Science, Anhui University, Hefei 230601, China*

<sup>3</sup>*Adaptive Networks and Control Laboratory, Department of Electronic Engineering,  
and the Center of Smart Networks and Systems,*

*School of Information Science and Engineering, Fudan University, Shanghai 200433, China*

<sup>4</sup>*School of Electrical, Computer and Energy Engineering,*

*Arizona State University, Tempe, Arizona 85287, USA*

<sup>5</sup>*Department of Communication Engineering, North University of China, Taiyuan, Shan'xi 030051, China*

(Dated: April 22, 2022)

In spite of the recent progress in data based inference of complex dynamical systems, to reconstruct cyberphysical systems with a multiplex network structure is an outstanding and challenging problem. We articulate a mean-field based maximum likelihood estimation framework to address this problem. For prototypical complex networks with a double layer structure and hosting spreading dynamics, we show that the structures of both cyber and physical layers can be simultaneously reconstructed from time series data. In addition to validating the framework using empirical and synthetic cyberphysical networks, we carry out a detailed analysis to elucidate the impacts of network and dynamics parameters on the reconstruction accuracy and robustness.

Data based reconstruction of complex networked systems has been an active area of research with broad applications, but previous works focused exclusively on single layer networks [1–30]. Many real world complex networked systems, especially cyberphysical systems [31] that have been a frontier field of interdisciplinary research, possess a multiplex structure: such a system typically comprises multiple interconnected network layers, each with a distinct type of connection pattern [32–36]. In view of the ubiquity of multiplex cyberphysical systems in many fields of science and engineering, the problem of reconstructing the full topology of the system based solely on data is well defined with broad applications. To our knowledge, so far this problem has not been investigated.

In this work, we develop a reconstruction framework based on mean-field maximum likelihood estimation to address the problem of data based reconstruction of multiplex networks. To demonstrate the general principle underlying our reconstruction framework in a concrete manner, we focus on a class of double layer cyberphysical systems. In such a system, there are two network layers, where the physical layer hosts epidemic spreading dynamics, e.g., susceptible-infected-susceptible (SIS) process, while the cyber layer is essentially a social network with information spreading governed by the unaware-aware-unaware (UAU) process [37]. Provided that binary time series data are available from both layers, we show, using empirical and synthetic networks, that our framework is capable of accurately reconstructing the full topology of each layer. We study the impacts of network structural and dynamics parameters on the reconstruction accuracy, such as the average degree, interlayer coupling, heterogeneous spreading rates, and noise. Our

framework represents an initial success to assess the “internal gear” of complex cyberphysical networked systems with a duplex structure, which can be generalized to more sophisticated multiplex systems with broad applications.

Cyberphysical systems with UAU-SIS coupled dynamics describe realistic situations where there is competition between disease spreading and social awareness, with the physical contact layer supporting an epidemic process and the virtual contact cyber-layer generating awareness diffusion. The duplex structure stipulates that all nodes represent the same individuals in the cyber and physical layers, but their connectivities are different. In the cyber layer, spreading of awareness can be described by an SIS process: an unaware node (U) can be informed by an aware neighbor (A) with probability  $\lambda$ , and the aware node can lose awareness and returns to the U state with probability  $\delta$ . The epidemic dynamics in the physical layer are also of the SIS type, where an infected (I) node can infect its susceptible (S) neighbors with a certain probability  $\beta$ , and the I-node returns to the S state with probability  $\mu$ . The dynamical interaction or coupling between the cyber and physical layers can be described, as follows. An I-node in the physical layer is automatically aware of the infection and changes to the A state immediately in the cyber layer. If one S-node is in the A state, its infectivity is discounted by a factor  $0 \leq \gamma < 1$ . A detailed model description and a schematic illustration of the UAU-SIS coupled dynamics are given in Sec. I and Fig. 4 of Supplementary Information (SI) [38], respectively.

To facilitate an understanding of the principle underlying our reconstruction framework, we introduce the mathematical notation  ${}_{x_4}^{x_3} X_{x_1}^{x_2}$  associated with a variable  $X$ , where  $x_1$  and  $x_2$  are the time attribute and the id number of  $X$  (e.g.,  $x_1 = t$  and  $x_2 = i$ ),  $x_3$  determines whether  $X$  belongs to the cyber layer (i.e.,  $x_3 = 1$ ) or the physical contact layer (i.e.,  $x_3 = 2$ ),  $x_4$  specifies ei-

\* haifengzhang1978@gmail.com

ther U or A. For example,  ${}_U\beta$  and  ${}_A\beta = \gamma \cdot {}_U\beta$  denote the infectivity rate of an unaware and an aware S-node, respectively. Variable  $s$  with three annotations denotes the state of a node, e.g.,  ${}^1s_{t_m}^i = 0$  or 1 ( ${}^2s_{t_m}^i = 0$  or 1) indicates that node  $i$  in the cyber (physical) layer is in U or A state (S or I state) at time  $t_m$ . Our framework can deal with the general case where the transmission and/or recovery rates are heterogeneous among the nodes (Sec. X in SI [38]).

For a cyberphysical system hosting UAU-SIS dynamics, at any time a node can be in one of the three distinct states: unaware and susceptible (US), aware and susceptible (AS), or aware and infected (AI). The state UI (unaware and infected) is redundant because an I-node becomes aware immediately. The connections of node  $i$  in the cyber and physical layers are recorded by the vectors  $\mathbf{a}^i$  and  $\mathbf{b}^i$ , respectively, where  $a_j^i = 1$  specifies that node  $j$  is a neighbor of node  $i$  in the cyber layer and  $a_j^i = 0$  otherwise, and  $b_j^i$  is defined similarly. The numbers of A-neighbors in the cyber layer and I-neighbors in the physical layer are  $\sum_{j \neq i} a_j^i {}^1s_t^j$  and  $\sum_{j \neq i} b_j^i {}^2s_t^j$ , respectively. In the absence of dynamical correlation, the relevant probabilities are  $r_t^i = (1 - \lambda^i) \sum_{j \neq i} a_j^i {}^1s_t^j$ ,  ${}_U q_t^i = (1 - {}_U \beta^i) \sum_{j \neq i} b_j^i {}^2s_t^j$

and  ${}_A q_t^i = (1 - {}_A \beta^i) \sum_{j \neq i} b_j^i {}^2s_t^j$ , where  $r_t^i$  is the probability that node  $i$  is not informed by any neighbor,  ${}_U q_t^i$  and  ${}_A q_t^i$  are the probabilities that node  $i$  is not infected by any neighbor if it was in the U state and A state, respectively. The transition probabilities for node  $i$  to be in the US, AS and AI states at the next time step under the condition that node  $i$  is in US state at time  $t$  are (from the tree of transition probabilities in Fig. 5 in SI [38])  $P^{US \rightarrow US} = r_t^i {}_U q_t^i$ ,  $P^{US \rightarrow AS} = (1 - r_t^i) {}_U q_t^i$  and  $P^{US \rightarrow AI} = 1 - {}_U q_t^i$ , respectively. Additional transition probabilities are:  $P^{AS \rightarrow US} = \delta^i {}_A q_t^i$ ,  $P^{AS \rightarrow AS} = (1 - \delta^i) {}_A q_t^i$ ,  $P^{AS \rightarrow AI} = 1 - {}_A q_t^i$ ,  $P^{AI \rightarrow US} = \delta^i \mu^i$ ,  $P^{AI \rightarrow AS} = (1 - \delta^i) \mu^i$  and  $P^{AI \rightarrow AI} = 1 - \mu^i$  (Sec. II of SI [38]).

Only the states  ${}^1s_{t_m}^i$  and  ${}^2s_{t_m}^i$  ( $i = 1, \dots, N$ ) at time  $t_m$  (not necessarily uniform) are recorded, where  $N$  is the network size. Our framework consists of three steps: (1) to reconstruct the likelihood function of the coupled dynamics, (2) to apply the mean-field approximation to enable maximum likelihood estimation (MLE), and (3) to transform the MLE problem into two solvable linear systems - one for each layer with solutions representing the neighbors of each node in the layer. In particular, the likelihood function of node  $i$  is given by (Sec. III of SI [38]):

$$\begin{aligned} & P \left( \left\{ {}^1s_{t_m+1}^i, {}^2s_{t_m+1}^i \right\}_{m=1 \dots M} \mid \left\{ {}^1s_{t_m}^j, {}^2s_{t_m}^j \right\}_{j=1 \dots N, m=1 \dots M}, \mathbf{a}^i, \mathbf{b}^i, \lambda^i, {}_U \beta^i, {}_A \beta^i, \delta^i, \mu^i \right) \\ &= \prod_m \left[ (r_{t_m}^i {}_U q_{t_m}^i)^{\left(1 - {}^1s_{t_m+1}^i\right) \left(1 - {}^2s_{t_m+1}^i\right)} ((1 - r_{t_m}^i) {}_U q_{t_m}^i)^{{}^1s_{t_m+1}^i \left(1 - {}^2s_{t_m+1}^i\right)} (1 - {}_U q_{t_m}^i)^{{}^1s_{t_m+1}^i {}^2s_{t_m+1}^i} \right]^{\left(1 - {}^1s_{t_m}^i\right) \left(1 - {}^2s_{t_m}^i\right)} \\ & \quad \left[ (\delta^i {}_A q_{t_m}^i)^{\left(1 - {}^1s_{t_m+1}^i\right) \left(1 - {}^2s_{t_m+1}^i\right)} ((1 - \delta^i) {}_A q_{t_m}^i)^{{}^1s_{t_m+1}^i \left(1 - {}^2s_{t_m+1}^i\right)} (1 - {}_A q_{t_m}^i)^{{}^1s_{t_m+1}^i {}^2s_{t_m+1}^i} \right]^{{}^1s_{t_m}^i \left(1 - {}^2s_{t_m}^i\right)} \\ & \quad \left[ (\delta^i \mu^i)^{\left(1 - {}^1s_{t_m+1}^i\right) \left(1 - {}^2s_{t_m+1}^i\right)} ((1 - \delta^i) \mu^i)^{{}^1s_{t_m+1}^i \left(1 - {}^2s_{t_m+1}^i\right)} (1 - \mu^i)^{{}^1s_{t_m+1}^i {}^2s_{t_m+1}^i} \right]^{{}^1s_{t_m}^i {}^2s_{t_m}^i}, \end{aligned} \quad (1)$$

where  $M$  is the length of the time series (step 1). The logarithmic form of Eq. (1) [denoted as  $L = L(a^i, b^i, \lambda^i, {}_U \beta^i, {}_A \beta^i, \delta^i, \mu^i)$ ] can be written as  $L = L_0(\delta^i, \mu^i) + L_1(\mathbf{a}^i, \lambda^i) + L_2(\mathbf{b}^i, {}_U \beta^i, {}_A \beta^i)$ . MLE can be performed by maximizing  $L_0$ ,  $L_1$  and  $L_2$  (Sec. III of SI [38]). Because  $L_0$  does not contain information about the network structure, it is only necessary to maximize  $L_1$  and  $L_2$  with respect to  $a_j^i$  and  $b_j^i$ , respectively. The likelihood function for reconstructing the cyber layer is (see Sec. V of SI [38] for the corresponding function and the detailed reconstruction process for the physical layer)

$$\begin{aligned} L_1(\mathbf{a}^i, \lambda^i) &= \sum_m {}^1X_{t_m}^i \ln \left( (1 - \lambda^i)^{\sum_{j \neq i} a_j^i {}^1s_{t_m}^j} \right) \quad (2) \\ &+ \sum_m {}^1Y_{t_m}^i \ln \left( 1 - (1 - \lambda^i)^{\sum_{j \neq i} a_j^i {}^1s_{t_m}^j} \right) \end{aligned}$$

where  ${}^1X_{t_m}^i = (1 - {}^1s_{t_m}^i) (1 - {}^1s_{t_m+1}^i)$  and  ${}^1Y_{t_m}^i = (1 - {}^1s_{t_m}^i) (1 - {}^2s_{t_m+1}^i) {}^1s_{t_m+1}^i$ .

The maximum value of  $L_1$  cannot be obtained straightforwardly by setting zero its derivative with respect to  $a_j^i$ , because  $a_j^i$  appears in the exponential term and the values of  $\lambda^i$  are unknown. We resort to the mean-field approximation to solve this problem (step 2). Specifically, for node  $i$  in the cyber layer, the fraction of A-neighbors ( $\sum_{j \neq i} {}^1s_{t_m}^j a_j^i$ ) is approximately equal to the fraction of A-nodes in the whole layer excluding node  $i$  itself:

$$\sum_{j \neq i} {}^1s_{t_m}^j a_j^i \approx \frac{{}^1k^i}{N-1} {}^1\theta_{t_m}^i, \quad (3)$$

where  ${}^1k^i$  is the degree of node  $i$ ,  ${}^1\theta_{t_m}^i = \sum_{j \neq i} {}^1s_{t_m}^j$  is the number of A-nodes excluding node  $i$  itself. Letting

${}^1\gamma^i = (1 - \lambda^i)^{\frac{1}{N-1}}$ , we rewrite Eq. (2) concisely as

$$\hat{L}_1({}^1\gamma^i) = \sum_m \left[ {}^1X_{t_m}^i \ln \left( ({}^1\gamma^i)^{{}^1\theta_{t_m}^i} \right) + {}^1Y_{t_m}^i \ln \left( 1 - ({}^1\gamma^i)^{{}^1\theta_{t_m}^i} \right) \right]. \quad (4)$$

Differentiating  $\hat{L}_1({}^1\gamma^i)$  with respect to  ${}^1\gamma^i$  and setting it to zero, we get the equation  $\sum_m {}^1Y_{t_m}^i {}^1\theta_{t_m}^i \frac{({}^1\gamma^i)^{{}^1\theta_{t_m}^i}}{1 - ({}^1\gamma^i)^{{}^1\theta_{t_m}^i}} = \sum_m {}^1X_{t_m}^i {}^1\theta_{t_m}^i$ , whose solutions give the values of  ${}^1\gamma^i$  denoted as  ${}^1\gamma^i = {}^1\tilde{\gamma}^i$ .

To transform the MLE problem into a linear system (step 3), we take the derivative of Eq. (2) with respect to  $a_l^i$  and set it to zero, which gives the following high-dimensional nonlinear equation:

$$\sum_m {}^1Y_{t_m}^i {}^1s_{t_m}^l \frac{(1 - \lambda^i)^{\sum_j a_j^i} {}^1s_{t_m}^j}{1 - (1 - \lambda^i)^{\sum_j a_j^i}} = \sum_m {}^1X_{t_m}^i {}^1s_{t_m}^l.$$

To obtain a solution, we take advantage of Eq. (3) and use first-order approximation. The result is a solvable linear system expressed in the matrix form  $\mathbf{\Lambda} \cdot \boldsymbol{\eta} = \boldsymbol{\zeta}$ , with vector  $\boldsymbol{\eta} = [a_1^i \ln(1 - \lambda^i), \dots, a_{i-1}^i \ln(1 - \lambda^i), a_{i+1}^i \ln(1 - \lambda^i), \dots, a_N^i \ln(1 - \lambda^i)]^T$  (see Sec. IV of SI [38] for the detailed forms of  $\mathbf{\Lambda}$  and  $\boldsymbol{\zeta}$ ). With the available time series  ${}^1s_{t_m}^i$  and  ${}^2s_{t_m}^i$ , the values of the elements of the matrix  $\mathbf{\Lambda}$  and the components of the vector  $\boldsymbol{\zeta}$  can be calculated, so the vector  $\boldsymbol{\eta}$  characterizing the connectivity of node  $i$  can be solved. Because  $\ln(1 - \lambda^i) < 0$  is a constant, the value of  $-a_l^i \ln(1 - \lambda^i)$  is much above zero for  $a_l^i = 1$  or close to zero for  $a_l^i = 0$ . A threshold value can then be readily set to distinguish the existent from the nonexistent links: a pair of nodes  $i$  and  $l$  are connected in the cyber layer if the value of  $-a_l^i \ln(1 - \lambda^i)$  is larger than the threshold (see Sec. VII of SI [38] for the criterion to choose the threshold).

We first validate our framework using an empirical network with 61 nodes, the so-called CS-AARHUS network [39]. The original network has five layers, but we regard the Facebook layer as the cyber layer and the other four off-line layers (Leisure, Work, Co-authorship, Lunch) as the physical layer, as illustrated in Figs. 1(a) and 1(b), respectively. Figures 1(c,d) show the values of  $-a_l^i \ln(1 - \lambda^i)$  and  $-b_l^i \ln(1 - \lambda^i)$  for the cyber and physical layers, respectively, where the blue and orange dots denote the existent and nonexistent links, respectively, which are well separated and can be unequivocally distinguished through a properly chosen threshold (Fig. 6 in SI [38]). For the physical layer in Fig. 1(d), the gap between the blue and orange dots decrease with the nodal degree. The reason that the neighbors of a larger degree node are harder to be detected is due to neighborhood overlapping, a result that is consistent with previous findings [25, 40]. For the cyber layer [Fig. 1(c)], the blue and orange dots for node 7 are overlapped even though  ${}^1k^7 = 6$ , but there is a finite gap for large degree nodes,

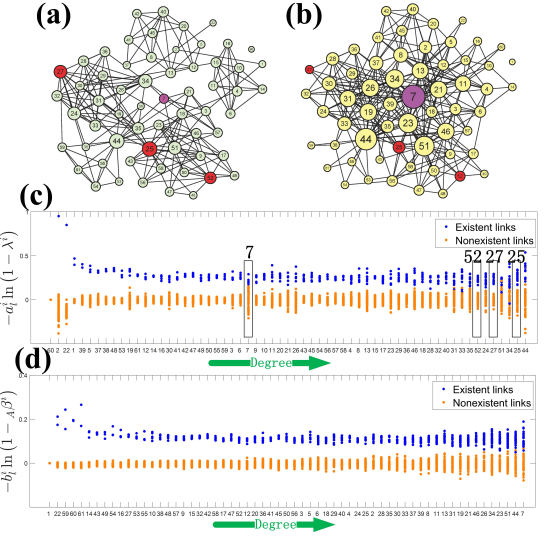


FIG. 1. Reconstruction of CS-AARHUS network. (a) Actual structure of the virtual contact (cyber) layer (Facebook). (b) The structure of the physical layer. (c,d) The values of  $-a_l^i \ln(1 - \lambda^i)$ ,  $i \neq l$  and  $-b_l^i \ln(1 - \lambda^i)$ ,  $i \neq l$ , respectively, versus the nodal degree. Each column gives the connectivity of a node, where the blue and orange dots denote the existent and nonexistent links, respectively. The length of time series  $M = 30000$ . The dynamics parameters are  $\lambda = 0.2$ ,  $u\beta = 0.2$ ,  $A\beta = 0.5u\beta$ , and  $\mu = \delta = 0.8$ .

e.g., node 52 with  ${}^1k^{52} = 10$ , node 27 with  ${}^1k^{27} = 12$ , and node 25 with  ${}^1k^{25} = 15$ . The relatively small gap of  ${}^1k^7$  can be understood that the counterpart value in the physical layer is large:  ${}^2k^7 = 29$ , indicating that the node is infected and is thus constantly in the A state in the cyber layer (an infected node becomes aware immediately). As a result, the states of the neighbors of this node in the cyber layer has little influence on its state, making reconstruction difficult. For nodes with large and small degrees in the cyber and physical layers, respectively, the transition from U to A state is mainly determined by the states of the neighbors, facilitating reconstruction. In general, the structure of the physical layer has a significant effect on the reconstruction of the cyber layer, but effect in the opposite direction is minimal.

We next demonstrate the power of our reconstruction framework for two additional empirical networks: *C. elegans* [36] and the innovation diffusion network for physicians (the so-called CKM network) [41]. Originally, both networks have three layers, and we choose the first layer as the cyber layer and the second layer as the physical layer. The top and bottom panels of Fig. 2 illustrate the reconstruction accuracy (measured by characterizing quantities AUROC, AUPR and success rate defined in Sec. VI of SI [38]) versus the time series length for the *C. elegans* and CKM networks, respectively, where longer time series result in better reconstruction performance, and the reconstruction accuracy of the physical layer is higher than that of the cyber layer, which are results that

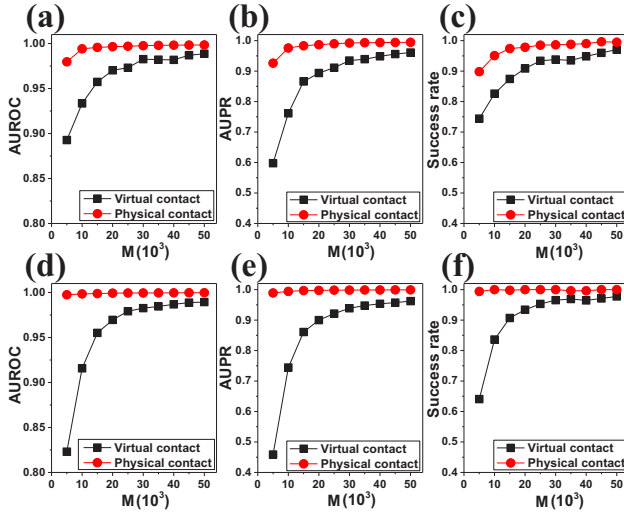


FIG. 2. Reconstruction accuracy of *C. elegans* and CKM networks. (a-c) Values of AUROC, AUPR and success rate versus the time series length  $M$ , respectively, for the *C. elegans* network, for the parameter setting  $\lambda = 0.2$ ,  $u\beta = 0.3$ ,  $A\beta = 0.5u\beta$ , and  $\mu = \delta = 0.8$ . (d-f) The corresponding results for the CKM network for the same parameter values as for (a-c) except  $u\beta = 0.5$ .

are consistent with those in Fig. 1.

How does network structural parameters such as the average degree affect the reconstruction accuracy? Figure 3(a) shows that an increase in the average degree  $\langle k_2 \rangle$  of the physical layer can greatly reduce the reconstruction accuracy of the cyber layer. Figures 3(b,c) show that, for the physical layer, the accuracy gradually decreases with its average degree, for a fixed average degree of the cyber layer. An explanation is that the probability of being infected tends to increase for a larger value of  $\langle k_1 \rangle$ , “hiding” the information required for uncovering the structure of the cyber layer. We also find that increasing the average degree  $\langle k_1 \rangle$  of the cyber layer tends to reduce the reconstruction accuracy of itself [Fig. 3(c)] but has a negligible effect on the reconstruction of the physical layer [Fig. 3(d)].

We test different types of model complex networks to gain insights into the effect of interlayer coupling on the reconstruction performance (Sec. IX in SI [38]). The general result is that the introduction of the physical layer can reduce the reconstruction accuracy of the cyber layer, but the latter can have a beneficial effect on the reconstruction of the former. We also test the effect of noise on reconstruction, with the result that noise (e.g., random state flipping) has a significant impact on the reconstruction of the cyber layer, but it hardly affects the

reconstruction of the physical layer (Sec. X in SI [38]).

To summarize, we develop a mean-field based maximum likelihood estimation framework to solve the open problem of data based reconstruction of cyberphysical networks with a double-layer structure. Using spreading as prototypical dynamical processes on both layers, we

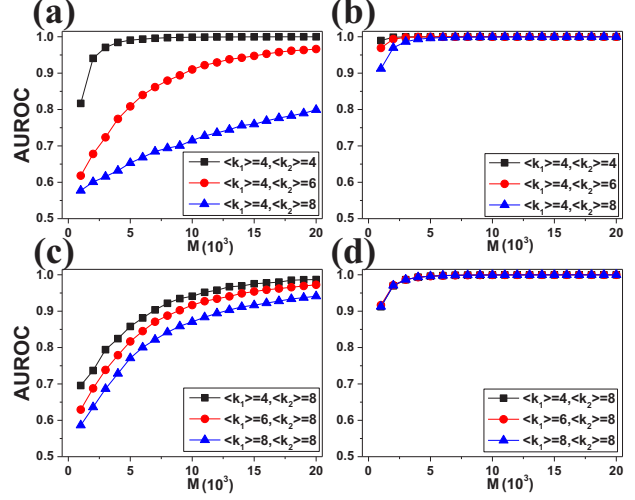


FIG. 3. Effect of average degree on reconstruction as measured by the AUROC index. (a,b) For a fixed value of the average degree  $\langle k_1 \rangle$  of the cyber layer, the effect of varying the average degree  $\langle k_2 \rangle$  of the physical layer on the reconstruction accuracy of the former and latter, respectively. (c,d) For a fixed value of  $\langle k_2 \rangle$ , the effect of varying the value of  $\langle k_1 \rangle$  on the reconstruction accuracy of the cyber and physical layer, respectively. Random double-layer networks with  $N=100$  are used. The parameters are  $\lambda = 0.3$ ,  $u\beta = 0.4$ ,  $A\beta = 0.5u\beta$ , and  $\mu = \delta = 0.8$ .

demonstrate the power of the framework through empirical and synthetic networks, and investigate the effects of physical factors such as the average degree, interlayer coupling, and noise on reconstruction. The main phenomenon is that the reconstruction accuracy of the physical layer is generally much higher than that of the cyber layer. Cyberphysical systems are becoming increasingly ubiquitous and pervasive in the modern society. Our work represents an initial step forward in addressing the challenging inverse or reverse engineering problem of these systems.

This work was supported by NSFC under Grant Nos. 61473001 and 11331009. YCL is supported by ONR through Grant No. N00014-16-1-2828. XL is supported by the National Science Fund for Distinguished Young Scholars of China (No. 61425019) and NSFC under Grant No. 71731004.

Supplementary Information for  
**Data based reconstruction of complex cyberphysical networks**

Chuang Ma, Han-Shuang Chen, Xiang Li, Ying-Cheng Lai, and Hai-Feng Zhang

**CONTENTS**

I. UAU-SIS dynamics on cyberphysical networks with a double-layer structure	6
II. Transition tree of UAU-SIS model	6
III. Likelihood function	8
IV. Reconstruction of cyber layer	9
V. Reconstruction of physical layer	10
VI. Metrics for performance characterization	13
VII. Selection of threshold value for identification of existent links	14
VIII. Reconstruction of double-layer networks with heterogeneous rates of spreading dynamics	14
IX. Effect of interlayer coupling on reconstruction accuracy	14
X. Effect of noise on reconstruction	14
References	14

## I. UAU-SIS DYNAMICS ON CYBERPHYSICAL NETWORKS WITH A DOUBLE-LAYER STRUCTURE

The UAU-SIS model was originally articulated [36] to study the competition between social awareness and disease spreading on double layer networks, where the physical contact layer supports an epidemic process and the virtual contact layer supports awareness diffusion [37]. The two layers share exactly the same set of nodes but their connection patterns are different. Spreading of awareness in the virtual layer is described by the conventional SIS dynamics: an unaware node (U) is informed by an aware neighbor (A) with probability  $\lambda$ , and an aware node can lose awareness and returns to the U state with probability  $\delta$ . Epidemic dynamics in the physical layer are also of the SIS type, where an infected (I) node can infect its susceptible (S) neighbors with probability  $\beta$ , and an I-node returns to the S state with probability  $\mu$ . The interlayer interaction can be described, as follows. An I-node in the physical layer is automatically aware of the infection and changes to the A state immediately in the virtual layer. If an S-node is in the A state, its infectivity is discounted by a factor  $0 \leq \gamma < 1$ . Figure 4 presents a schematic illustration of the double layer network with the interacting dynamical processes as described.

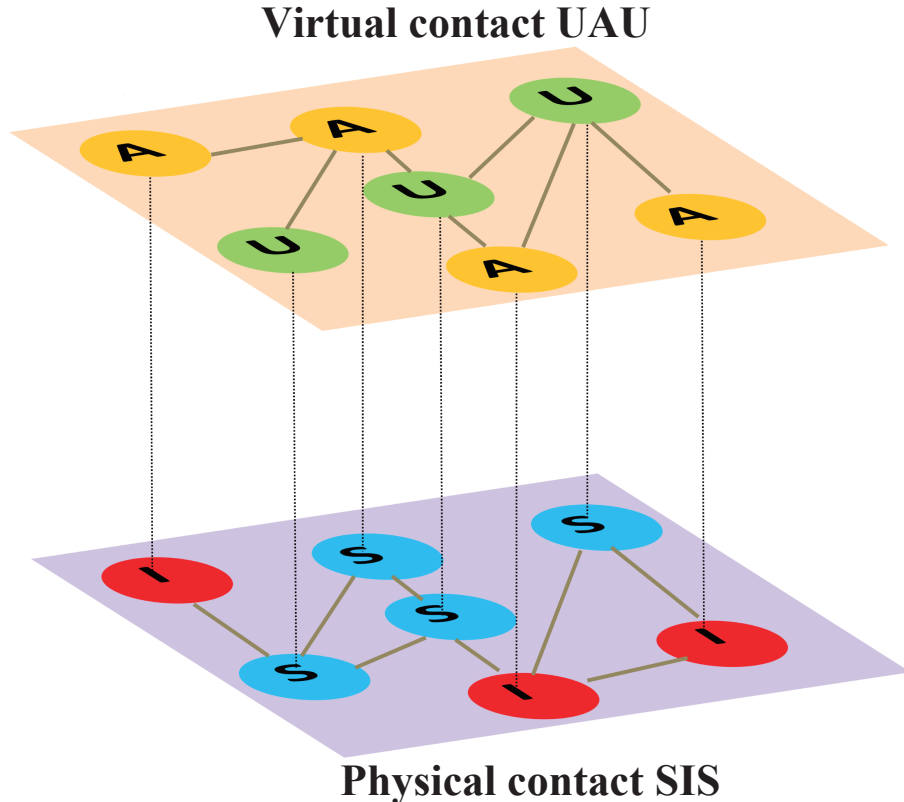


FIG. 4. **Schematic illustration a cyberphysical system with a double layer interacting structure.** The upper layer (cyber or virtual contact) supports awareness diffusion, in which nodes have two possible states: unaware (U) or aware (A). The bottom layer (physical contact) hosts epidemic spreading dynamics, where a node can be in the susceptible (S) or infected (I) state.

## II. TRANSITION TREE OF UAU-SIS MODEL

Let  ${}_U\beta$  and  ${}_A\beta = \gamma \cdot {}_U\beta$  be the infectivity rates of unaware and aware S-node, respectively. For node  $i$ ,  $\sum_{j \neq i} a_j^{i-1} s_t^j$  and  $\sum_{j \neq i} b_j^{i-2} s_t^j$  are the numbers of A-neighbors in the cyber layer and I-neighbors in the physical layer, respectively.

In the absence of dynamical correlation, the following probabilities are essential to the network spreading dynamics: (1)  $r_t^i$ , the probability that node  $i$  is not informed by any neighbor, (2)  ${}_U q_t^i$ , the probability that node  $i$  is not infected by any neighbor if  $i$  was unaware, and (3)  ${}_A q_t^i$ , the probability that node  $i$  is not infected by any neighbor if  $i$  was aware. These probabilities are given by

$$\begin{aligned} r_t^i &= (1 - \lambda^i)^{\sum_{j \neq i} a_j^{i,1} s_t^j}, \\ {}_U q_t^i &= (1 - U \beta^i)^{\sum_{j \neq i} b_j^{i,2} s_t^j}, \\ {}_A q_t^i &= (1 - A \beta^i)^{\sum_{j \neq i} b_j^{i,2} s_t^j}. \end{aligned} \quad (5)$$

A tacit assumption in Ref. [37] is that diffusion of awareness in the virtual layer occurs before epidemic spreading in the physical layer. In our work, we do not require that the two types of spreading dynamics occur in any particular order. Figure 5 presents the transition probability tree of the UAU-SIS coupling dynamics on the cyberphysical networks that we study.

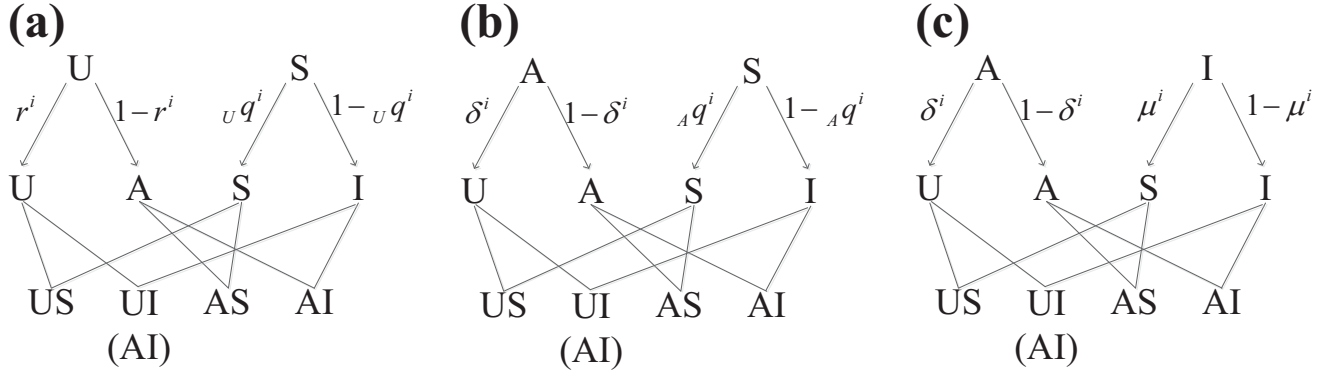


FIG. 5. **Transition probability tree of coupled UAU-SIS dynamics in cyberphysical networks with a double-layer structure.** The notations are: AI - aware and infected, UI - unaware and infected (redundant to the AI state), AS - aware and susceptible, and US - unaware and susceptible.

From Fig. 5 and Eq. (5), we have that the probabilities of node  $i$  being in the US, AS and AI states at  $t + 1$  when it is in the US state at time  $t$  are

$$\begin{aligned} P^{US \rightarrow US} &= r_t^i {}_U q_t^i, \\ P^{US \rightarrow AS} &= (1 - r_t^i) {}_U q_t^i, \\ P^{US \rightarrow AI} &= r_t^i (1 - {}_U q_t^i) + (1 - r_t^i) (1 - {}_U q_t^i) = 1 - {}_U q_t^i. \end{aligned} \quad (6)$$

The probabilities of node  $i$  being in the US, AS and AI states at  $t + 1$  when it is in the AS state at time  $t$  are

$$\begin{aligned} P^{AS \rightarrow US} &= \delta^i {}_A q_t^i, \\ P^{AS \rightarrow AS} &= (1 - \delta^i) {}_A q_t^i, \\ P^{AS \rightarrow AI} &= \delta^i (1 - {}_A q_t^i) + (1 - \delta^i) (1 - {}_A q_t^i) = 1 - {}_A q_t^i. \end{aligned} \quad (7)$$

The probabilities for node  $i$  to be in the US, AS and AI states at  $t + 1$  if it is in the AI state at time  $t$  are

$$\begin{aligned} P^{AI \rightarrow US} &= \delta^i {}_A q_t^i, \\ P^{AI \rightarrow AS} &= (1 - \delta^i) {}_A q_t^i, \\ P^{AI \rightarrow AI} &= \delta^i (1 - {}_A q_t^i) + (1 - \delta^i) (1 - {}_A q_t^i) = 1 - {}_A q_t^i. \end{aligned} \quad (8)$$

### III. LIKELIHOOD FUNCTION

The likelihood function of a node can be written in the following compact form:

$$P \left( \left\{ {}^1 s_{t_m+1}^i, {}^2 s_{t_m+1}^i \right\}_{m=1 \dots M} \mid \left\{ {}^1 s_{t_m}^j, {}^2 s_{t_m}^j \right\}_{j=1 \dots N, m=1 \dots M}, \mathbf{a}^i, \mathbf{b}^i, \lambda^i, {}_U \beta^i, {}_A \beta^i, \delta^i, \mu^i \right) \quad (9)$$

$$= \prod_m \left[ \left( r_{t_m}^i {}_U q_{t_m}^i \right)^{\left( 1 - {}^1 s_{t_m+1}^i \right) \left( 1 - {}^2 s_{t_m+1}^i \right)} \left( \left( 1 - r_{t_m}^i \right) {}_U q_{t_m}^i \right)^{{}^1 s_{t_m+1}^i \left( 1 - {}^2 s_{t_m+1}^i \right)} \left( 1 - {}_U q_{t_m}^i \right)^{{}^1 s_{t_m+1}^i {}^2 s_{t_m+1}^i} \right]^{\left( 1 - {}^1 s_{t_m}^i \right) \left( 1 - {}^2 s_{t_m}^i \right)}$$

$$\left[ \left( \delta^i {}_A q_{t_m}^i \right)^{\left( 1 - {}^1 s_{t_m+1}^i \right) \left( 1 - {}^2 s_{t_m+1}^i \right)} \left( \left( 1 - \delta^i \right) {}_A q_{t_m}^i \right)^{{}^1 s_{t_m+1}^i \left( 1 - {}^2 s_{t_m+1}^i \right)} \left( 1 - {}_A q_{t_m}^i \right)^{{}^1 s_{t_m+1}^i {}^2 s_{t_m+1}^i} \right]^{{}^1 s_{t_m}^i \left( 1 - {}^2 s_{t_m}^i \right)}$$

$$\left[ \left( \delta^i \mu^i \right)^{\left( 1 - {}^1 s_{t_m+1}^i \right) \left( 1 - {}^2 s_{t_m+1}^i \right)} \left( \left( 1 - \delta^i \right) \mu^i \right)^{{}^1 s_{t_m+1}^i \left( 1 - {}^2 s_{t_m+1}^i \right)} \left( 1 - \mu^i \right)^{{}^1 s_{t_m+1}^i {}^2 s_{t_m+1}^i} \right]^{{}^1 s_{t_m}^i {}^2 s_{t_m}^i}.$$

In our cyberphysical system, we assume that a node, once it is infected in the physical layer, enters into the A state immediately in the cyber layer:  ${}^2 s_t^i = 1$  indicates  ${}^1 s_t^i = 1$  at any time  $t$ . As a result, we have  ${}^1 s_{t_m}^i {}^2 s_{t_m}^i = {}^2 s_{t_m}^i$  and  ${}^1 s_{t_m+1}^i {}^2 s_{t_m+1}^i = {}^2 s_{t_m+1}^i$ . Note that a node in the U state in the cyber layer cannot be in the I state in the physical layer, i.e.,  ${}^1 s_t^i = 0$  indicates  ${}^2 s_t^i = 0$  at any time  $t$ , leading to

$$\begin{aligned} \left( 1 - {}^1 s_{t_m}^i \right) \left( 1 - {}^2 s_{t_m}^i \right) &= 1 - {}^1 s_{t_m}^i \quad \text{and} \\ \left( 1 - {}^1 s_{t_m+1}^i \right) \left( 1 - {}^2 s_{t_m+1}^i \right) &= 1 - {}^1 s_{t_m+1}^i. \end{aligned}$$

Equation (9) appears complicated, but it can be reduced to some simple form. For example, assuming that node  $i$  at  $t_m$  is in the US state:  ${}^1 s_{t_m}^i = 0$  and  ${}^2 s_{t_m}^i = 0$ , we need to retain only one term in the product:

$$\left[ \left( r_{t_m}^i {}_U q_{t_m}^i \right)^{\left( 1 - {}^1 s_{t_m+1}^i \right) \left( 1 - {}^2 s_{t_m+1}^i \right)} \left( \left( 1 - r_{t_m}^i \right) {}_U q_{t_m}^i \right)^{{}^1 s_{t_m+1}^i \left( 1 - {}^2 s_{t_m+1}^i \right)} \left( 1 - {}_U q_{t_m}^i \right)^{{}^1 s_{t_m+1}^i {}^2 s_{t_m+1}^i} \right],$$

which can be further reduced to  $\left( 1 - r_{t_m}^i \right) {}_U q_{t_m}^i$  if  ${}^1 s_{t_m+1}^i = 1$  and  ${}^2 s_{t_m+1}^i = 0$  (i.e., in the AS state at the next time step). This corresponds to the transition probability from the US state to the AS state:  $P^{US \rightarrow AS} = \left( 1 - r_t^i \right) {}_U q_t^i$  in Eq. (6). In general, Eq. (9) contains all the transition probabilities in Eqs. (6)-(8).

After some algebra, we obtain the logarithmic form of Eq. (9) as

$$L \left( \mathbf{a}^i, \mathbf{b}^i, \lambda^i, {}_U \beta^i, {}_A \beta^i, \delta^i, \mu^i \right) = L_0 \left( \delta^i, \mu^i \right) + L_1 \left( \mathbf{a}^i, \lambda^i \right) + L_2 \left( \mathbf{b}^i, {}_U \beta^i, {}_A \beta^i \right), \quad (10)$$

where

$$L_0 \left( \delta^i, \mu^i \right) = \sum_m \left[ \begin{aligned} {}^1 s_{t_m}^i \left( 1 - {}^1 s_{t_m+1}^i \right) \ln \left( \delta^i \right) + {}^1 s_{t_m}^i {}^1 s_{t_m+1}^i \left( 1 - {}^2 s_{t_m+1}^i \right) \ln \left( 1 - \delta^i \right) \\ + {}^2 s_{t_m}^i \left( 1 - {}^2 s_{t_m+1}^i \right) \ln \left( \mu^i \right) + {}^2 s_{t_m}^i {}^2 s_{t_m+1}^i \ln \left( 1 - \mu^i \right) \end{aligned} \right]. \quad (11)$$

Note that Eq. (11) does not rely on any information about the network structure. The quantity that does contain the information is  $L_1 \left( \mathbf{a}^i, \lambda^i \right)$ , which depends on the connectivity of node  $i$  in the cyber layer. It can be written as

$$L_1 \left( \mathbf{a}^i, \lambda^i \right) = \sum_m \left[ {}^1 X_{t_m}^i \ln \left( \left( 1 - \lambda^i \right) \sum_{j \neq i} {}^a_j {}^1 s_{t_m}^j \right) + {}^1 Y_{t_m}^i \ln \left( 1 - \left( 1 - \lambda^i \right) \sum_{j \neq i} {}^a_j {}^1 s_{t_m}^j \right) \right], \quad (12)$$

where

$$\begin{aligned} {}^1 X_{t_m}^i &= \left( 1 - {}^1 s_{t_m}^i \right) \left( 1 - {}^1 s_{t_m+1}^i \right) \quad \text{and} \\ {}^1 Y_{t_m}^i &= \left( 1 - {}^1 s_{t_m}^i \right) \left( 1 - {}^2 s_{t_m+1}^i \right) {}^1 s_{t_m+1}^i. \end{aligned}$$

Similarly, the quantity  $L_2 \left( \mathbf{b}^i, {}_U \beta^i, {}_A \beta^i \right)$  that depends on the connectivity of node  $i$  in the physical layer is given by

$$\begin{aligned} L_2 \left( \mathbf{b}^i, {}_U \beta^i, {}_A \beta^i \right) &= \sum_m \left[ {}^2 {}_U X_{t_m}^i \ln \left( \left( 1 - {}_U \beta^i \right) \sum_{j \neq i} {}^b_j {}^2 s_{t_m}^j \right) + {}^2 {}_U Y_{t_m}^i \ln \left( 1 - \left( 1 - {}_U \beta^i \right) \sum_{j \neq i} {}^b_j {}^2 s_{t_m}^j \right) \right] \\ &+ \sum_m \left[ {}^2 {}_A X_{t_m}^i \ln \left( \left( 1 - {}_A \beta^i \right) \sum_{j \neq i} {}^b_j {}^2 s_{t_m}^j \right) + {}^2 {}_A Y_{t_m}^i \ln \left( 1 - \left( 1 - {}_A \beta^i \right) \sum_{j \neq i} {}^b_j {}^2 s_{t_m}^j \right) \right] \end{aligned} \quad (13)$$

where

$$\begin{aligned} {}^2_U X_{t_m}^i &= (1 - {}^1 s_{t_m}^i) (1 - {}^2 s_{t_m+1}^i), \\ {}^2_U Y_{t_m}^i &= (1 - {}^1 s_{t_m}^i) {}^2 s_{t_m+1}^i, \\ {}^2_A X_{t_m}^i &= {}^1 s_{t_m}^i (1 - {}^2 s_{t_m}^i) (1 - {}^2 s_{t_m+1}^i), \text{ and} \\ {}^2_A Y_{t_m}^i &= {}^1 s_{t_m}^i (1 - {}^2 s_{t_m}^i) {}^2 s_{t_m+1}^i. \end{aligned}$$

In principle, Eq. (10) indicates that one can maximize  $L_1$  and  $L_2$  with respect to  $a_j^i$  and  $b_j^i$ , respectively, to uncover the connectivity of node  $i$ . However, the conventional maximization process leads to equations that cannot be solved because the quantity  $a_j^i$  ( $b_j^i$ ) appears in the exponential term and the values of  $\lambda^i$  (or  $U\beta^i$ ) are unknown. We exploit the mean-field approximation to maximize  $L_1$  and  $L_2$ .

#### IV. RECONSTRUCTION OF CYBER LAYER

To infer the neighbors of node  $i$  in the cyber layer, we impose the mean-field approximation on  $L_1$ :

$$\sum_{j \neq i} {}^1 s_{t_m}^j a_j^i \approx \frac{{}^1 k^i}{N-1} {}^1 \theta_{t_m}^i, \quad (14)$$

where  $N$  and  ${}^1 k^i$  are the number of nodes and the degree of node  $i$  in the cyber layer, respectively, and the number of A-nodes in the cyber layer (excluding node  $i$  itself) is  ${}^1 \theta_{t_m}^i = \sum_{j \neq i} {}^1 s_{t_m}^j$ . A new unknown parameter  ${}^1 k^i$  emerges in Eq. (12) when we substitute Eq. (14) into Eq. (12). To simplify the analysis, we let

$${}^1 \gamma^i = (1 - \lambda^i)^{\frac{{}^1 k^i}{N-1}}, \quad (15)$$

to obtain

$$(1 - \lambda^i)^{\sum_{j \neq i} a_j^i} {}^1 s_{t_m}^j = (1 - \lambda^i)^{\frac{{}^1 k^i}{N-1} {}^1 \theta_{t_m}^i} = ({}^1 \gamma^i)^{{}^1 \theta_{t_m}^i}.$$

Equation (12) can then be written concisely as

$$\hat{L}_1 ({}^1 \gamma^i) = \sum_m \left[ {}^1 X_{t_m}^i \ln \left( ({}^1 \gamma^i)^{{}^1 \theta_{t_m}^i} \right) + {}^1 Y_{t_m}^i \ln \left( 1 - ({}^1 \gamma^i)^{{}^1 \theta_{t_m}^i} \right) \right]. \quad (16)$$

Differentiating  $\hat{L}_1 ({}^1 \gamma^i)$  with respect to  ${}^1 \gamma^i$  and setting it to zero, we get

$$\sum_m {}^1 Y_{t_m}^i {}^1 \theta_{t_m}^i \frac{({}^1 \gamma^i)^{{}^1 \theta_{t_m}^i}}{1 - ({}^1 \gamma^i)^{{}^1 \theta_{t_m}^i}} = \sum_m {}^1 X_{t_m}^i {}^1 \theta_{t_m}^i,$$

leading to  ${}^1 \gamma^i = {}^1 \tilde{\gamma}^i$ .

Treating  $a_l^i$  as a continuous variance, we can further differentiate Eq. (12) with respect to  $a_l^i$  and set it to zero, which gives

$$\sum_m {}^1 Y_{t_m}^i {}^1 s_{t_m}^l \frac{(1 - \lambda^i)^{\sum_{j \neq i} a_j^i} {}^1 s_{t_m}^j}{1 - (1 - \lambda^i)^{\sum_{j \neq i} a_j^i} {}^1 s_{t_m}^j} = \sum_m {}^1 X_{t_m}^i {}^1 s_{t_m}^l. \quad (17)$$

To obtain analytical solutions of Eq. (17) is not feasible due to its nonlinear and high-dimensional nature. We thus resort to first-order Taylor expansion. In particular, we expand  $a^x/(1 - a^x)$  in the limit  $x \rightarrow x_0$  to obtain

$$\frac{a^x}{1 - a^x} \approx \frac{a^{x_0}}{1 - a^{x_0}} + \frac{a^{x_0} \ln a}{(1 - a^{x_0})^2} (x - x_0) = \frac{a^{x_0}}{1 - a^{x_0}} - \frac{a^{x_0} \ln a^{x_0}}{(1 - a^{x_0})^2} + \frac{a^{x_0} \ln a}{(1 - a^{x_0})^2} x. \quad (18)$$

Setting  $x = \sum_{j \neq i} a_j^i {}^1 s_{t_m}^j$ ,  $a = 1 - \lambda^i$ , and  $x_0 = \frac{{}^1 k^i}{N-1} {}^1 \theta_{t_m}^i$  [Eq. (14) implies that  $x \approx x_0$ ], we have

$$a^{x_0} = ({}^1 \tilde{\gamma}^i)^{{}^1 \theta_{t_m}^i}$$

from Eq. (15). That is, the term

$$\frac{(1 - \lambda^i)^{\sum_{j \neq i} a_j^{i-1} s_{t_m}^j}}{1 - (1 - \lambda^i)^{\sum_{j \neq i} a_j^{i-1} s_{t_m}^j}}$$

in Eq. (17) can be expressed as a linear form based on Eq. (14.)

Collecting all the approximations, we transform Eq. (17) into a solvable linear system as

$$\sum_m {}^1 Y_{t_m}^i {}^1 G_{t_m}^i {}^1 s_{t_m}^l \ln(1 - \lambda^i) \sum_{j \neq i} a_j^{i-1} s_{t_m}^j = \sum_m ({}^1 X_{t_m}^i - {}^1 Y_{t_m}^i {}^1 F_{t_m}^i) {}^1 s_{t_m}^l, \quad (19)$$

where

$$\begin{aligned} {}^1 F_{t_m}^i &= \frac{({}^1 \tilde{\gamma}^i)^{1 \theta_{t_m}^i}}{1 - ({}^1 \tilde{\gamma}^i)^{1 \theta_{t_m}^i}} - \frac{({}^1 \tilde{\gamma}^i)^{1 \theta_{t_m}^i}}{\left(1 - ({}^1 \tilde{\gamma}^i)^{1 \theta_{t_m}^i}\right)^2} {}^1 \theta_{t_m}^i \ln {}^1 \tilde{\gamma}^i \quad \text{and} \\ {}^1 G_{t_m}^i &= \frac{({}^1 \tilde{\gamma}^i)^{1 \theta_{t_m}^i}}{\left(1 - ({}^1 \tilde{\gamma}^i)^{1 \theta_{t_m}^i}\right)^2}. \end{aligned}$$

Setting  ${}^1 \Phi_{t_m}^i = {}^1 Y_{t_m}^i {}^1 G_{t_m}^i$  and  ${}^1 \Gamma_{t_m}^i = {}^1 X_{t_m}^i - {}^1 Y_{t_m}^i {}^1 F_{t_m}^i$ , we express Eq. (19) as

$$\begin{bmatrix} \sum_m {}^1 \Phi_{t_m}^i {}^1 s_{t_m}^1 {}^1 s_{t_m}^1 & \dots & \sum_m {}^1 \Phi_{t_m}^i {}^1 s_{t_m}^1 {}^1 s_{t_m}^{i-1} & \sum_m {}^1 \Phi_{t_m}^i {}^1 s_{t_m}^1 {}^1 s_{t_m}^{i+1} & \dots & \sum_m {}^1 \Phi_{t_m}^i {}^1 s_{t_m}^1 {}^1 s_{t_m}^N \\ \vdots & & \vdots & \vdots & & \vdots \\ \sum_m {}^1 \Phi_{t_m}^i {}^1 s_{t_m}^{i-11} {}^1 s_{t_m}^1 & \dots & \sum_m {}^1 \Phi_{t_m}^i {}^1 s_{t_m}^{i-11} {}^1 s_{t_m}^{i-1} & \sum_m {}^1 \Phi_{t_m}^i {}^1 s_{t_m}^{i-11} {}^1 s_{t_m}^{i+1} & \dots & \sum_m {}^1 \Phi_{t_m}^i {}^1 s_{t_m}^{i-11} {}^1 s_{t_m}^N \\ \sum_m {}^1 \Phi_{t_m}^i {}^1 s_{t_m}^{i+11} {}^1 s_{t_m}^1 & \dots & \sum_m {}^1 \Phi_{t_m}^i {}^1 s_{t_m}^{i+11} {}^1 s_{t_m}^{i-1} & \sum_m {}^1 \Phi_{t_m}^i {}^1 s_{t_m}^{i+11} {}^1 s_{t_m}^{i+1} & \dots & \sum_m {}^1 \Phi_{t_m}^i {}^1 s_{t_m}^{i+11} {}^1 s_{t_m}^N \\ \vdots & & \vdots & \vdots & & \vdots \\ \sum_m {}^1 \Phi_{t_m}^i {}^1 s_{t_m}^N {}^1 s_{t_m}^1 & \dots & \sum_m {}^1 \Phi_{t_m}^i {}^1 s_{t_m}^N {}^1 s_{t_m}^{i-1} & \sum_m {}^1 \Phi_{t_m}^i {}^1 s_{t_m}^N {}^1 s_{t_m}^{i+1} & \dots & \sum_m {}^1 \Phi_{t_m}^i {}^1 s_{t_m}^N {}^1 s_{t_m}^N \end{bmatrix} \times \begin{bmatrix} a_1^i \ln(1 - \lambda^i) \\ \vdots \\ a_{i-1}^i \ln(1 - \lambda^i) \\ a_{i+1}^i \ln(1 - \lambda^i) \\ \vdots \\ a_N^i \ln(1 - \lambda^i) \end{bmatrix} = \begin{bmatrix} \sum_m {}^1 \Gamma_{t_m}^i {}^1 s_{t_m}^1 \\ \vdots \\ \sum_m {}^1 \Gamma_{t_m}^i {}^1 s_{t_m}^{i-1} \\ \sum_m {}^1 \Gamma_{t_m}^i {}^1 s_{t_m}^{i+1} \\ \vdots \\ \sum_m {}^1 \Gamma_{t_m}^i {}^1 s_{t_m}^N \end{bmatrix}. \quad (20)$$

The matrix on the left side (labeled as  $\Lambda$ ) and the vector (labeled as  $\zeta$ ) on the right side of Eq. (20) can be calculated from the time series of the nodal states. The vector

$$\boldsymbol{\eta} = [a_1^i \ln(1 - \lambda^i), \dots, a_{i-1}^i \ln(1 - \lambda^i), a_{i+1}^i \ln(1 - \lambda^i), \dots, a_N^i \ln(1 - \lambda^i)]^T$$

can then be solved, where  $T$  denotes transpose. Note that the quantity  $\ln(1 - \lambda^i) < 0$  is a constant even though  $\lambda^i$  is not given, implying that the value of  $-a_j^i \ln(1 - \lambda^i)$  is positively large for  $a_j^i = 1$  and near zero for  $a_j^i = 0$ . As a result, the neighbors of node  $i$  in the cyber layer can be ascertained through the solution of vector  $\boldsymbol{\eta}$ .

## V. RECONSTRUCTION OF PHYSICAL LAYER

The mean-field approximation for the physical layer is

$$\sum_{j \neq i} {}^2 s_{t_m}^j b_j^i \approx \frac{2k^i}{N-1} {}^2 \theta_{t_m}^i, \quad (21)$$

where  ${}^2k^i$  is the degree of node  $i$  and  ${}^2\theta_{t_m}^i = \sum_{j \neq i} {}^2s_{t_m}^j$  is the number of I-nodes in the physical layer (excluding node  $i$  itself). We set

$$\begin{aligned} {}^2_U\gamma^i &= (1 - {}_U\beta^i)^{\frac{2k^i}{N-1}} \text{ and} \\ {}^2_A\gamma^i &= (1 - {}_A\beta^i)^{\frac{2k^i}{N-1}} \end{aligned} \quad (22)$$

and write Eq. (13) concisely as

$$\hat{L}_2({}^2_U\gamma^i, {}^2_A\gamma^i) = \sum_m \left\{ \begin{aligned} & \left[ {}^2_U X_{t_m}^i \ln \left( ({}^2_U\gamma^i)^{\frac{2\theta_{t_m}^i}{N-1}} \right) + {}^2_U Y_{t_m}^i \ln \left( 1 - ({}^2_U\gamma^i)^{\frac{2\theta_{t_m}^i}{N-1}} \right) \right] \\ & + \left[ {}^2_A X_{t_m}^i \ln \left( ({}^2_A\gamma^i)^{\frac{2\theta_{t_m}^i}{N-1}} \right) + {}^2_A Y_{t_m}^i \ln \left( 1 - ({}^2_A\gamma^i)^{\frac{2\theta_{t_m}^i}{N-1}} \right) \right] \end{aligned} \right\}. \quad (23)$$

Taking the derivatives of  $\hat{L}_2$  with respect to  ${}^2_U\gamma^i$  and  ${}^2_A\gamma^i$  and setting them to zero, we get

$$\sum_m {}^2_U Y_{t_m}^i {}^2\theta_{t_m}^i \frac{({}^2_U\gamma^i)^{\frac{2\theta_{t_m}^i}{N-1}}}{1 - ({}^2_U\gamma^i)^{\frac{2\theta_{t_m}^i}{N-1}}} = \sum_m {}^2_U X_{t_m}^i {}^2\theta_{t_m}^i \quad (24)$$

and

$$\sum_m {}^2_A Y_{t_m}^i {}^2\theta_{t_m}^i \frac{({}^2_A\gamma^i)^{\frac{2\theta_{t_m}^i}{N-1}}}{1 - ({}^2_A\gamma^i)^{\frac{2\theta_{t_m}^i}{N-1}}} = \sum_m {}^2_A X_{t_m}^i {}^2\theta_{t_m}^i, \quad (25)$$

which give

$$\begin{aligned} {}^2_U\gamma^i &= {}^2_U\tilde{\gamma}^i \text{ and} \\ {}^2_A\gamma^i &= {}^2_A\tilde{\gamma}^i. \end{aligned}$$

Similar to the mean-field analysis of the cyber layer, we differentiate Eq. (13) with respect to  $b_l^i$  and set it to zero:

$$\begin{aligned} \frac{\partial L_2}{\partial b_l^i} &= \sum_m \left[ \ln(1 - {}_U\beta^i) {}^2_U X_{t_m}^i {}^2s_{t_m}^l - \ln(1 - {}_U\beta^i) {}^2_U Y_{t_m}^i {}^2s_{t_m}^l \frac{(1 - {}_U\beta^i)^{\sum_j b_j^i {}^2s_{t_m}^j}}{1 - (1 - {}_U\beta^i)^{\sum_j b_j^i {}^2s_{t_m}^j}} \right] \\ &+ \sum_m \left[ \ln(1 - {}_A\beta^i) {}^2_A X_{t_m}^i {}^2s_{t_m}^l - \ln(1 - {}_A\beta^i) {}^2_A Y_{t_m}^i {}^2s_{t_m}^l \frac{(1 - {}_A\beta^i)^{\sum_j b_j^i {}^2s_{t_m}^j}}{1 - (1 - {}_A\beta^i)^{\sum_j b_j^i {}^2s_{t_m}^j}} \right] = 0, \end{aligned}$$

which gives

$$\begin{aligned} & \sum_m \left\{ \ln(1 - {}_U\beta^i) {}^2s_{t_m}^l {}^2_U Y_{t_m}^i \frac{(1 - {}_U\beta^i)^{\sum_j b_j^i {}^2s_{t_m}^j}}{1 - (1 - {}_U\beta^i)^{\sum_j b_j^i {}^2s_{t_m}^j}} + \ln(1 - {}_A\beta^i) {}^2s_{t_m}^l {}^2_A Y_{t_m}^i \frac{(1 - {}_A\beta^i)^{\sum_j b_j^i {}^2s_{t_m}^j}}{1 - (1 - {}_A\beta^i)^{\sum_j b_j^i {}^2s_{t_m}^j}} \right\} \\ &= \sum_m \{ \ln(1 - {}_U\beta^i) {}^2_U X_{t_m}^i {}^2s_{t_m}^l + \ln(1 - {}_A\beta^i) {}^2_A X_{t_m}^i {}^2s_{t_m}^l \}. \end{aligned} \quad (26)$$

Setting

$$\rho = \frac{\ln {}^2_U\tilde{\gamma}^i}{\ln {}^2_A\tilde{\gamma}^i} = \frac{\ln(1 - {}_U\beta^i)}{\ln(1 - {}_A\beta^i)},$$

we can further simplify Eq. (26) as

$$\begin{aligned} & \sum_m \left[ \rho {}^2s_{t_m}^l {}^2_U Y_{t_m}^i \frac{(1 - {}_U\beta^i)^{\sum_j b_j^i {}^2s_{t_m}^j}}{1 - (1 - {}_U\beta^i)^{\sum_j b_j^i {}^2s_{t_m}^j}} + {}^2s_{t_m}^l {}^2_A Y_{t_m}^i \frac{(1 - {}_A\beta^i)^{\sum_j b_j^i {}^2s_{t_m}^j}}{1 - (1 - {}_A\beta^i)^{\sum_j b_j^i {}^2s_{t_m}^j}} \right] \\ &= \sum_m [\rho {}^2_U X_{t_m}^i {}^2s_{t_m}^l + {}^2_A X_{t_m}^i {}^2s_{t_m}^l] \end{aligned} \quad (27)$$

Using Eq. (18) and setting  $x = \sum_{j \neq i} b_j^i {}^2 s_{t_m}^j$  and  $x_0 = \frac{2k^i}{N-1} {}^2 \theta_{t_m}^i$ , we obtain the following Taylor expansion:

$$\frac{(1 - {}_U \beta^i) \sum_{j \neq i} b_j^i {}^2 s_{t_m}^j}{1 - (1 - {}_U \beta^i) \sum_{j \neq i} b_j^i {}^2 s_{t_m}^j} = {}_U^2 F_{t_m}^i + {}_U^2 G_{t_m}^i \ln (1 - {}_U \beta^i) \sum_{j \neq i} b_j^i {}^2 s_{t_m}^j, \quad (28)$$

where

$$\begin{aligned} {}_U^2 F_{t_m}^i &= \frac{({}_U^2 \tilde{\gamma}^i)^{2 \theta_{t_m}^i}}{1 - ({}_U^2 \tilde{\gamma}^i)^{2 \theta_{t_m}^i}} - \frac{({}_U^2 \tilde{\gamma}^i)^{2 \theta_{t_m}^i}}{\left(1 - ({}_U^2 \tilde{\gamma}^i)^{2 \theta_{t_m}^i}\right)^2} {}^2 \theta_{t_m}^i \ln {}_U^2 \tilde{\gamma}^i \text{ and} \\ {}_U^2 G_{t_m}^i &= \frac{({}_U^2 \tilde{\gamma}^i)^{2 \theta_{t_m}^i}}{\left(1 - ({}_U^2 \tilde{\gamma}^i)^{2 \theta_{t_m}^i}\right)^2}. \end{aligned}$$

We also have

$$\frac{(1 - {}_A \beta^i) \sum_{j \neq i} b_j^i {}^2 s_{t_m}^j}{1 - (1 - {}_A \beta^i) \sum_{j \neq i} b_j^i {}^2 s_{t_m}^j} = {}_A^2 F_{t_m}^i + {}_A^2 G_{t_m}^i \ln (1 - {}_A \beta^i) \sum_{j \neq i} b_j^i {}^2 s_{t_m}^j, \quad (29)$$

where

$$\begin{aligned} {}_A^2 F_{t_m}^i &= \frac{({}_A^2 \tilde{\gamma}^i)^{2 \theta_{t_m}^i}}{1 - ({}_A^2 \tilde{\gamma}^i)^{2 \theta_{t_m}^i}} - \frac{({}_A^2 \tilde{\gamma}^i)^{2 \theta_{t_m}^i}}{\left(1 - ({}_A^2 \tilde{\gamma}^i)^{2 \theta_{t_m}^i}\right)^2} {}^2 \theta_{t_m}^i \ln {}_A^2 \tilde{\gamma}^i \text{ and} \\ {}_A^2 G_{t_m}^i &= \frac{({}_A^2 \tilde{\gamma}^i)^{2 \theta_{t_m}^i}}{\left(1 - ({}_A^2 \tilde{\gamma}^i)^{2 \theta_{t_m}^i}\right)^2}. \end{aligned}$$

With these approximations, we can transform Eq. (27) into the following linear system:

$$\begin{aligned} &\sum_m \left[ \left( \rho {}_U^2 Y_{t_m}^i {}_U^2 G_{t_m}^i + {}_A^2 Y_{t_m}^i {}_A^2 G_{t_m}^i \right) {}^2 s_{t_m}^l \ln (1 - {}_A \beta^i) \sum_{j \neq i} b_j^i {}^2 s_{t_m}^j \right] \\ &= \sum_m \left( \rho {}_U^2 X_{t_m}^i + {}_A^2 X_{t_m}^i - \rho {}_U^2 Y_{t_m}^i {}_U^2 F_{t_m}^i - {}_A^2 Y_{t_m}^i {}_A^2 F_{t_m}^i \right) {}^2 s_{t_m}^l, \end{aligned} \quad (30)$$

where

$$\begin{aligned} {}^2 \Phi_{t_m}^i &= \rho {}_U^2 Y_{t_m}^i {}_U^2 G_{t_m}^i + {}_A^2 Y_{t_m}^i {}_A^2 G_{t_m}^i \text{ and} \\ {}^2 \Gamma_{t_m}^i &= \rho {}_U^2 X_{t_m}^i + {}_A^2 X_{t_m}^i - \rho {}_U^2 Y_{t_m}^i {}_U^2 F_{t_m}^i - {}_A^2 Y_{t_m}^i {}_A^2 F_{t_m}^i. \end{aligned}$$

We rewrite Eq. (30) in the following matrix form:

$$\begin{bmatrix}
 \sum_m 2\Phi_{t_m}^i 2s_{t_m}^1 2s_{t_m}^1 \dots \sum_m 2\Phi_{t_m}^i 2s_{t_m}^1 2s_{t_m}^{i-1} \sum_m 2\Phi_{t_m}^i 2s_{t_m}^1 2s_{t_m}^{i+1} \dots \sum_m 2\Phi_{t_m}^i 2s_{t_m}^1 2s_{t_m}^N \\
 \vdots \vdots \vdots \vdots \\
 \sum_m 2\Phi_{t_m}^i 2s_{t_m}^{i-1} 2s_{t_m}^1 \dots \sum_m 2\Phi_{t_m}^i 2s_{t_m}^{i-1} 2s_{t_m}^{i-1} \sum_m 2\Phi_{t_m}^i 2s_{t_m}^{i-1} 2s_{t_m}^{i+1} \dots \sum_m 2\Phi_{t_m}^i 2s_{t_m}^{i-1} 2s_{t_m}^N \\
 \sum_m 2\Phi_{t_m}^i 2s_{t_m}^{i+1} 2s_{t_m}^1 \dots \sum_m 2\Phi_{t_m}^i 2s_{t_m}^{i+1} 2s_{t_m}^{i-1} \sum_m 2\Phi_{t_m}^i 2s_{t_m}^{i+1} 2s_{t_m}^{i+1} \dots \sum_m 2\Phi_{t_m}^i 2s_{t_m}^{i+1} 2s_{t_m}^N \\
 \vdots \vdots \vdots \vdots \\
 \sum_m 2\Phi_{t_m}^i 2s_{t_m}^N 2s_{t_m}^1 \dots \sum_m 2\Phi_{t_m}^i 2s_{t_m}^N 2s_{t_m}^{i-1} \sum_m 2\Phi_{t_m}^i 2s_{t_m}^N 2s_{t_m}^{i+1} \dots \sum_m 2\Phi_{t_m}^i 2s_{t_m}^N 2s_{t_m}^N
 \end{bmatrix} \\
 \times \begin{bmatrix}
 b_1^i \ln(1 - A\beta^i) \\
 \vdots \\
 b_{i-1}^i \ln(1 - A\beta^i) \\
 b_{i+1}^i \ln(1 - A\beta^i) \\
 \vdots \\
 b_N^i \ln(1 - A\beta^i)
 \end{bmatrix} = \begin{bmatrix}
 \sum_m 2\Gamma_{t_m}^i 2s_{t_m}^1 \\
 \vdots \\
 \sum_m 2\Gamma_{t_m}^i 2s_{t_m}^{i-1} \\
 \sum_m 2\Gamma_{t_m}^i 2s_{t_m}^{i+1} \\
 \vdots \\
 \sum_m 2\Gamma_{t_m}^i 2s_{t_m}^N
 \end{bmatrix}. \quad (31)$$

The matrix on the left side and the vector on the right side can be obtained from time series. Solution of Eq. (31) gives the vector

$$\boldsymbol{\xi} = [b_1^i \ln(1 - A\beta^i), \dots, b_{i-1}^i \ln(1 - A\beta^i), b_{i+1}^i \ln(1 - A\beta^i), \dots, b_N^i \ln(1 - A\beta^i)]^T,$$

revealing the neighbors of node  $i$  in the physical layer.

## VI. METRICS FOR PERFORMANCE CHARACTERIZATION

We use three metrics [42] to characterize the performance of our reconstruction framework: the area under the receiver operating characteristic curve (AUROC), the area under the precision-recall curve (AUPR), and the Success rate.

To define AUROC and AUPR, it is necessary to calculate three basic quantities: TPR (true positive rate), FPR (false positive rate), and Recall [42]. In particular, TPR is defined as

$$\text{TPR}(l) = \frac{\text{TP}(l)}{T}, \quad (32)$$

where  $l$  is the cut-off index in the list of the predicted links,  $\text{TP}(l)$  is the number of true positives in the top  $l$  predictions in the link list, and  $T$  is the number of positives.

FPR is defined as

$$\text{FPR}(l) = \frac{\text{FP}(l)}{Q}, \quad (33)$$

where  $\text{FP}(l)$  is the number of false positive in the top  $l$  entries in the predicted link list, and  $Q$  is the number of negatives by the golden standard.

Recall and Precision are defined as

$$\text{Recall}(l) = \text{TPR}(l) = \frac{\text{TP}(l)}{T}. \quad (34)$$

and

$$\text{Precision}(l) = \frac{\text{TP}(l)}{\text{TP}(l) + \text{FP}(l)} = \frac{\text{TP}(l)}{l}, \quad (35)$$

respectively.

Varying the value of  $l$  from 0 to  $N$ , we plot two sequences of points:  $[FPR(l), TPR(l)]$  and  $[Recall(l), Precision(l)]$ . The area under the two curves correspond to the values of AUROC and AUPR, respectively. For perfect reconstruction, we have AUROC=1 and AUPR=1. In the worst case (completely random), we have AUROC=0.5 and AUPR= $T/2N$ .

Let  $n_1$  and  $n_2$  be the numbers of the existent and nonexistent links in the network, respectively,  $n_3$  and  $n_4$  be the numbers of the predicted existent and nonexistent links. The Success rates for existent links (SREL) and nonexistent links (SRNL) are defined as  $n_3/n_1$  and  $n_4/n_2$ , respectively. The normalized Success rate is [25]  $\sqrt{SREL \times SRNL}$ .

## VII. SELECTION OF THRESHOLD VALUE FOR IDENTIFICATION OF EXISTENT LINKS

For each node  $i$ , the values of  $a_l^i \ln(1 - \lambda^i)$  (or of  $b_l^i \ln(1 - A\beta^i)$ ) can be solved with Eq. (20) [or Eq. (31)]. From Figs. 6(a,b), we have that the values of  $-a_l^i \ln(1 - \lambda^i)$  (or  $-b_l^i \ln(1 - A\beta^i)$ ) are unequivocally above zero for existent links, while their values are close to zero for nonexistent links, with a gap between the two sets of values. Representing the values listed in each column as a histogram, we have that the peak centered about zero corresponds to nonexistent links and the other corresponds to existent links. A threshold value can be placed between the two peaks, as shown in Fig. 6(c). A pair of nodes  $i$  and  $l$  are connected if the corresponding value of  $-a_l^i \ln(1 - \lambda^i)$  [ $-b_l^i \ln(1 - A\beta^i)$ ] is larger than the threshold. Take node 46 as an example. We wish to infer its neighbors in the physical layer [highlighted by the red dashed frame in Fig. 6(b)]. Figure 6(d) shows that the values larger than the threshold correspond to the existent links.

## VIII. RECONSTRUCTION OF DOUBLE-LAYER NETWORKS WITH HETEROGENEOUS RATES OF SPREADING DYNAMICS

Figure 7 demonstrates that our framework can reconstruct double-layer networks with heterogeneous rates of spreading dynamics. In particular, transmission rates  $\lambda^i$  and  $U\beta^i$  are randomly chosen from the ranges  $(0.2, 0.4)$  and  $(0.3, 0.5)$ , respectively. The recovery rates  $\delta^i$  and  $\mu^i$  are randomly from the ranges  $(0.6, 1)$  and  $(0.6, 1)$ , respectively. Note that  $A\beta^i = 0.5U\beta^i$ .

## IX. EFFECT OF INTERLAYER COUPLING ON RECONSTRUCTION ACCURACY

To understand the effect of interlayer coupling on the reconstruction performance, we test typical model complex networks: small-world (SW-SW) [43], Erdős-Rényi (ER-ER) [44], and Barabási-Albert (BA-BA) [45] double layer networks. For comparison, we include the special case where each layer is separately reconstructed without taking into account the other layer, which is equivalent to reconstructing a single-layer network (labeled as single). Figure 8 shows that the reconstruction accuracy of the cyber layer is greatly reduced when a physical layer is introduced (e.g., from blue to black traces). Without the physical layer, the transition of an unaware node in the cyber layer to the aware state depends only on the states of its neighbors. With the presence of the physical layer, an A-node can spontaneously become aware once it is infected, “concealing” the information about the structure of the cyber layer. On the contrary, the reconstruction accuracy of the physical layer can be improved slightly (e.g., from blue to red traces) when the cyber layer is introduced, which reduces the infectivity of A-nodes and prevents too many nodes from being in the I state, facilitating reconstruction. Figure 8 also illustrates that the reconstruction accuracy of the SW-SW network is better than that of the ER-ER random network and much better than that of the BA-BA network due to the difficulty in reconstructing the neighbors of the large degree nodes.

## X. EFFECT OF NOISE ON RECONSTRUCTION

Figure 9 shows the effect of noise on the reconstruction accuracy, where noise is implemented by randomly flipping a fraction  $\tau$  of the states among the total number  $MN$  of states. Noise has a significant effect on the reconstruction of the cyber layer, but it hardly affects the reconstruction of the physical layer (even when the flip rate is  $\tau \approx 20\%$ ).

---

[1] K. J. Friston, NeuroImage **16**, 513 (2002).

[2] T. S. Gardner, D. di Bernardo, D. Lorenz, and J. J. Collins, Science **301**, 102 (2003).

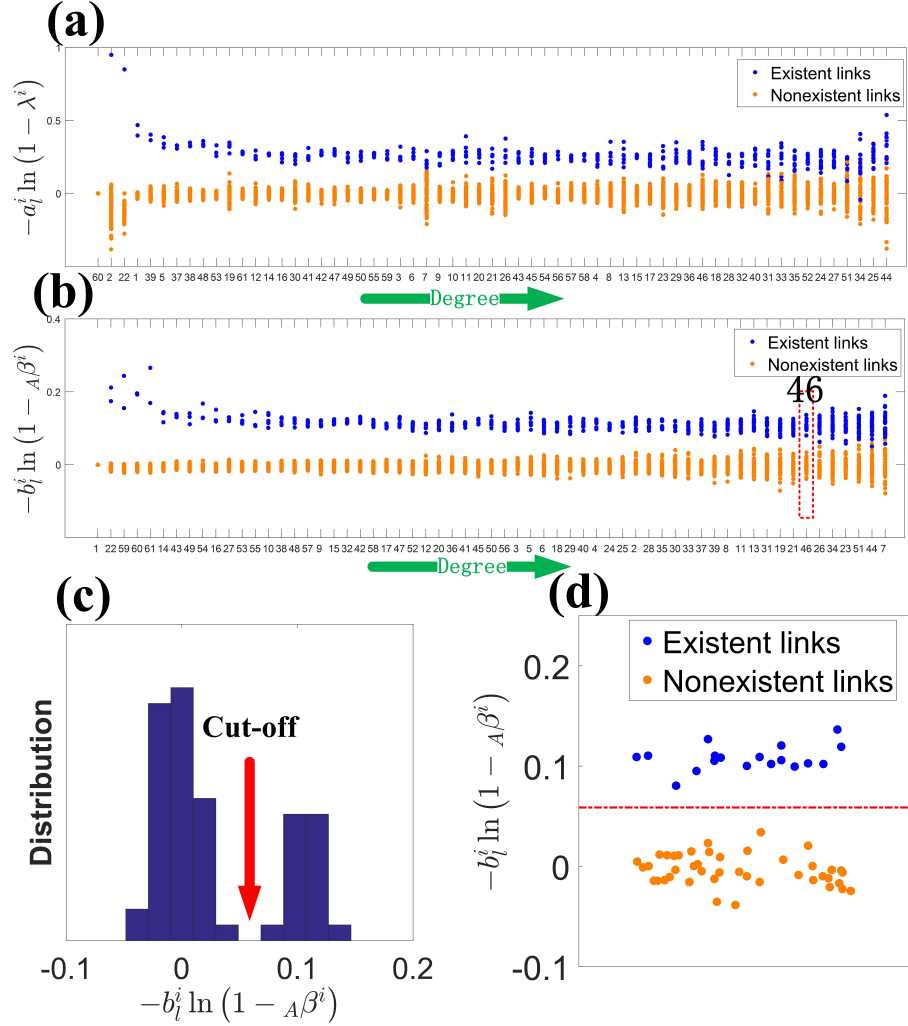


FIG. 6. **Reconstruction of CS-AARHUS double-layer network.** (a,b) Values of  $-a_l^i \ln(1 - \lambda^i)$ ,  $i \neq l$  and  $-b_l^i \ln(1 - \lambda^i)$   $i \neq l$  (b) for each node, respectively. Each column gives the connectivity of a node. The blue and orange points denote the existent and nonexistent links, respectively. (c) Illustration of the choice of the threshold with node 46 [highlighted by the red dashed frame in (b)]. Shown is the distribution of the values of  $-b_l^i \ln(1 - \lambda^i)$  for  $l \neq 46$ . The peak centered about zero corresponds to nonexistent links while the other peak corresponds to existent links. The threshold can be set within the gap between the two peaks. (d) The threshold is given to determine the nonexistent and existent links. The length of time series is  $M=30000$ . Other parameters are  $\lambda = 0.2$ ,  $U\beta = 0.2$ ,  $A\beta = 0.5U\beta$ , and  $\mu = \delta = 0.8$ .

- [3] G. Pipa and S. Grün, *Neurocomp.* **52**, 31 (2003).
- [4] A. Brovelli, M. Ding, A. Ledberg, Y. Chen, R. Nakamura, and S. L. Bressler, *Proc. Nat. Acad. Sci. (USA)* **101**, 9849 (2004).
- [5] V. M. Eguiluz, D. R. Chialvo, G. A. Cecchi, M. Baliki, and A. V. Apkarian, *Phys. Rev. Lett.* **94**, 018102 (2005).
- [6] D. Yu, M. Righero, and L. Kocarev, *Phys. Rev. Lett.* **97**, 188701 (2006).
- [7] J. Bongard and H. Lipson, *Proc. Natl. Acad. Sci. (USA)* **104**, 9943 (2007).
- [8] M. Timme, *Phys. Rev. Lett.* **98**, 224101 (2007).
- [9] D. Napoletani and T. D. Sauer, *Phys. Rev. E* **77**, 026103 (2008).
- [10] J. Donges, Y. Zou, N. Marwan, and J. Kurths, *EPL (Europhys. Lett.)* **87**, 48007 (2009).
- [11] S. Pajevic and D. Plenz, *PLoS Comp. Biol.* **5**, e1000271 (2009).
- [12] J. Ren, W.-X. Wang, B. Li, and Y.-C. Lai, *Phys. Rev. Lett.* **104**, 058701 (2010).
- [13] Z. Levnajić and A. Pikovsky, *Phys. Rev. Lett.* **107**, 034101 (2011).
- [14] S. Hempel, A. Koseska, J. Kurths, and Z. Nikoloski, *Phys. Rev. Lett.* **107**, 054101 (2011).
- [15] S. G. Shandilya and M. Timme, *New J. Phys.* **13**, 013004 (2011).
- [16] W.-X. Wang, Y.-C. Lai, C. Grebogi, and J.-P. Ye, *Phys. Rev. X* **1**, 021021 (2011).

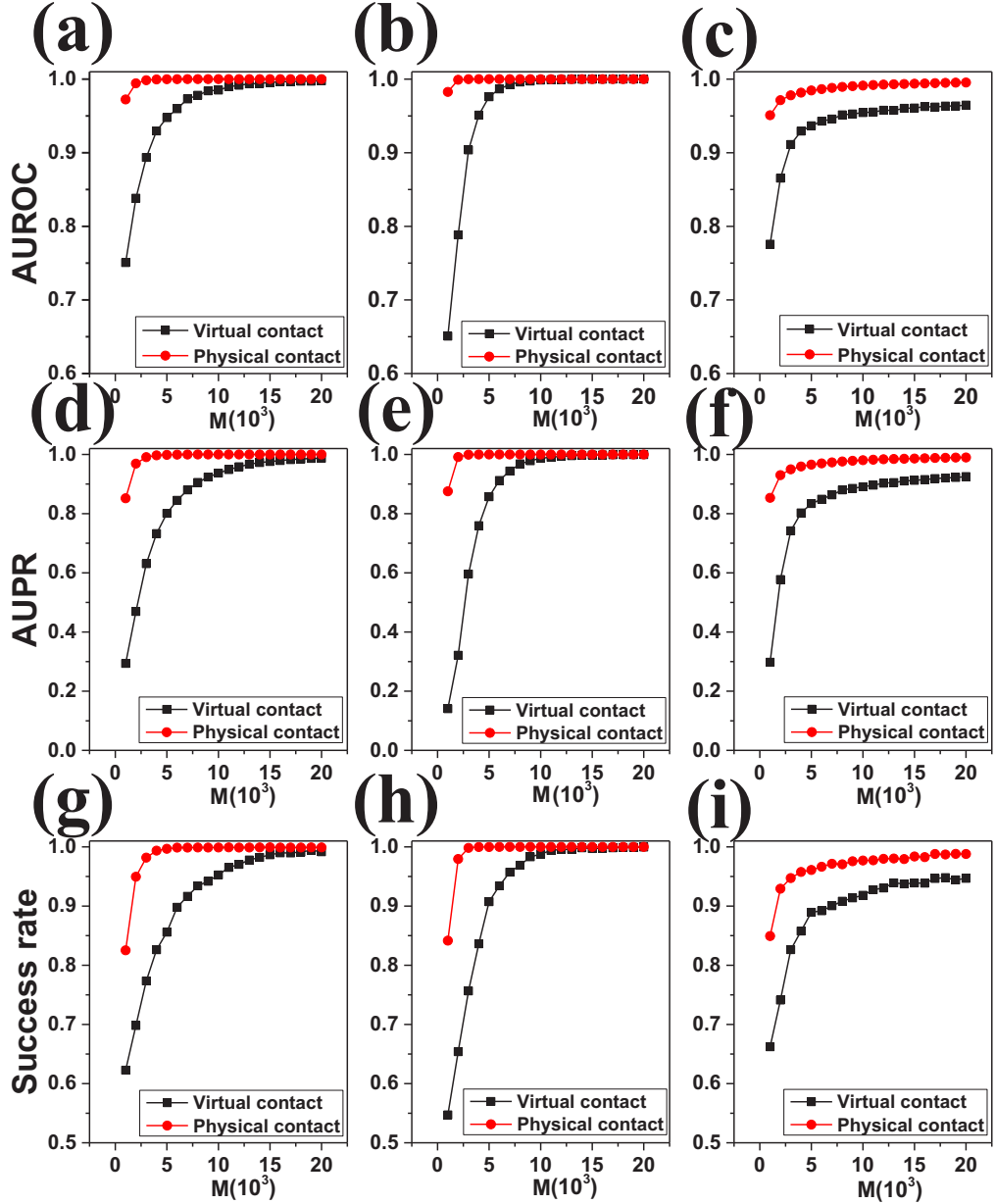


FIG. 7. **Applicability of reconstruction framework to spreading dynamics with heterogeneous rates.** Reconstruction accuracy versus the length  $M$  of the time series for ER-ER (left panel), SW-SW (central panel) and BA-BA (right panel) double-layer networks with heterogeneous transmission and recovery rates. The network parameters are  $N = 100$  and  $\langle k_1 \rangle = 4$ ,  $\langle k_2 \rangle = 6$ .

- [17] T. Berry, F. Hamilton, N. Peixoto, and T. Sauer, *J. Neurosci. Meth.* **209**, 388 (2012).
- [18] O. Stetter, D. Battaglia, J. Soriano, and T. Geisel, *PLoS Comp. Biol.* **8**, e1002653 (2012).
- [19] R.-Q. Su, W.-X. Wang, and Y.-C. Lai, *Phys. Rev. E* **85**, 065201 (2012).
- [20] F. Hamilton, T. Berry, N. Peixoto, and T. Sauer, *Phys. Rev. E* **88**, 052715 (2013).
- [21] D. Zhou, Y. Xiao, Y. Zhang, Z. Xu, and D. Cai, *Phys. Rev. Lett.* **111**, 054102 (2013).
- [22] E. S. C. Ching, P.-Y. Lai, and C. Y. Leung, *Phys. Rev. E* **88**, 042817 (2013).
- [23] M. Timme and J. Casadiego, *J. Phys. A. Math. Theo.* **47**, 343001 (2014).
- [24] R.-Q. Su, Y.-C. Lai, and X. Wang, *Entropy* **16**, 3889 (2014).
- [25] Z.-S. Shen, W.-X. Wang, Y. Fan, Z. Di, and Y.-C. Lai, *Nat. Commun.* **5**, 4323 (2014).
- [26] E. S. C. Ching, P.-Y. Lai, and C. Y. Leung, *Phys. Rev. E* **91**, 030801 (2015).
- [27] W.-X. Wang, Y.-C. Lai, and C. Grebogi, *Phys. Rep.* **644**, 1 (2016).

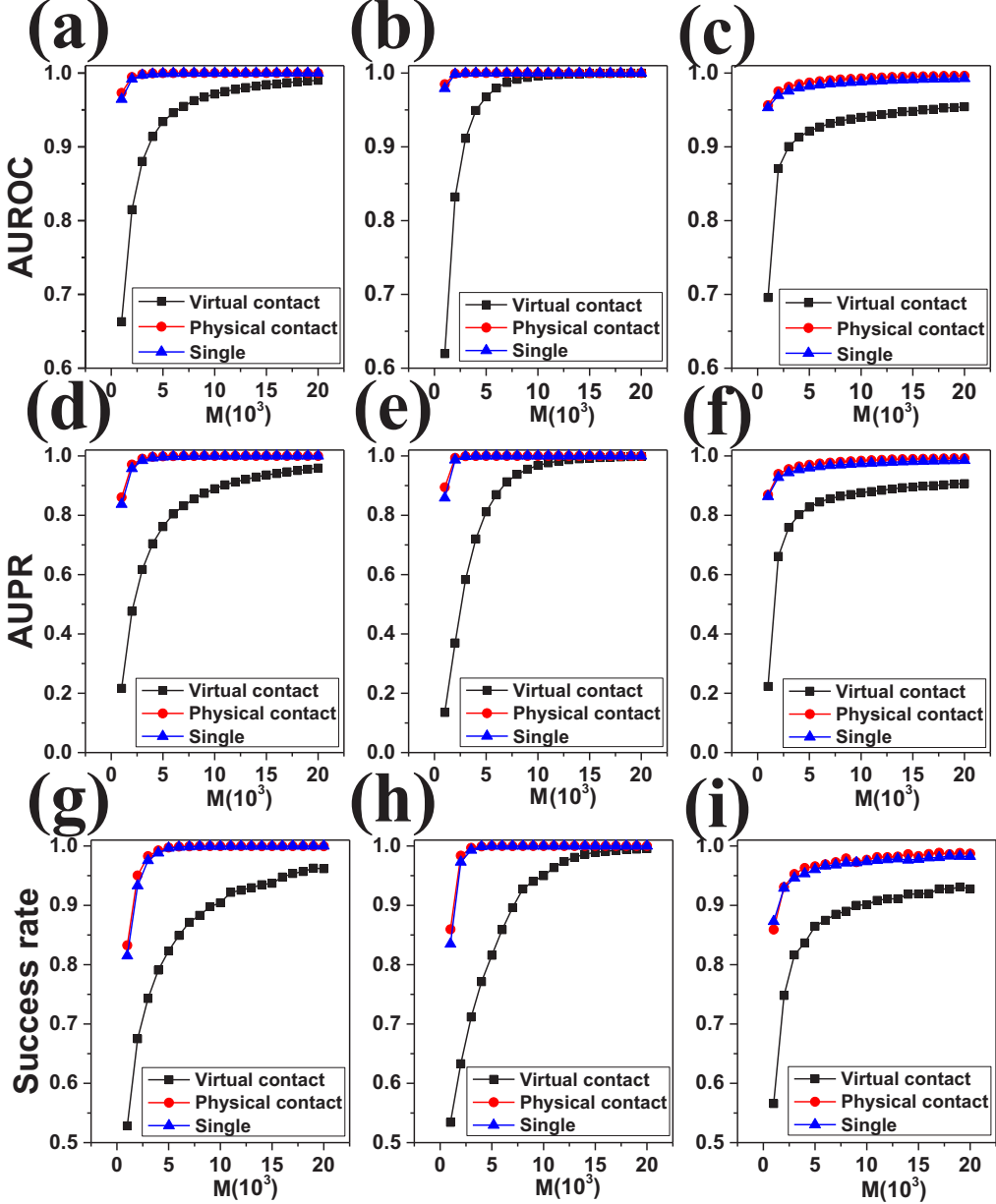


FIG. 8. Effect of interlayer coupling on reconstruction accuracy. Columns 1-3: reconstruction performance for ER-ER, SW-SW, and BA-BA double-layer networks, respectively. The “single” case indicates absence of interlayer coupling:  $u\beta = 0$  ( $\lambda = 0$ ) for the cyber (physical) layer. The parameter setting is  $\lambda = 0.4$ ,  $u\beta = 0.4$ ,  $A\beta = 0.5u\beta$ , and  $\mu = \delta = 0.8$ . The structures of the two layers are identical. The network parameters are  $N = 100$  and  $\langle k_1 \rangle = \langle k_2 \rangle = 6$ .

- [28] J. Casadiego, M. Nitzan, S. Hallerberg, and M. Timme, *Nat. Commun.* **8**, 2192 (2017).
- [29] X. Li and X. Li, *Nat. Commun.* **8**, 15729 (2017).
- [30] G. Mei, X. Wu, Y. Wang, M. Hu, J.-A. Lu, and G. Chen, *IEEE Trans. Cybernet* **48**, 754 (2018).
- [31] G. Wen, W. Yu, X. Yu, and J. Lü, *J. Sys. Sci. Complexity* **30**, 46 (2017).
- [32] S. V. Buldyrev, R. Parshani, G. Paul, H. E. Stanley, and S. Havlin, *Nature* **464**, 1025 (2010).
- [33] J. Gao, S. V. Buldyrev, H. E. Stanley, and S. Havlin, *Nat. Phys.* **8**, 40 (2012).
- [34] M. De Domenico, A. Solé-Ribalta, E. Cozzo, M. Kivelä, Y. Moreno, M. A. Porter, S. Gómez, and A. Arenas, *Phys. Rev. X* **3**, 041022 (2013).
- [35] M. Kivelä, A. Arenas, M. Barthelemy, J. P. Gleeson, Y. Moreno, and M. A. Porter, *J. Complex Net.* **2**, 203 (2014).
- [36] M. De Domenico, C. Granell, M. A. Porter, and A. Arenas, *Nat. Phys.* **12**, 901 (2016).

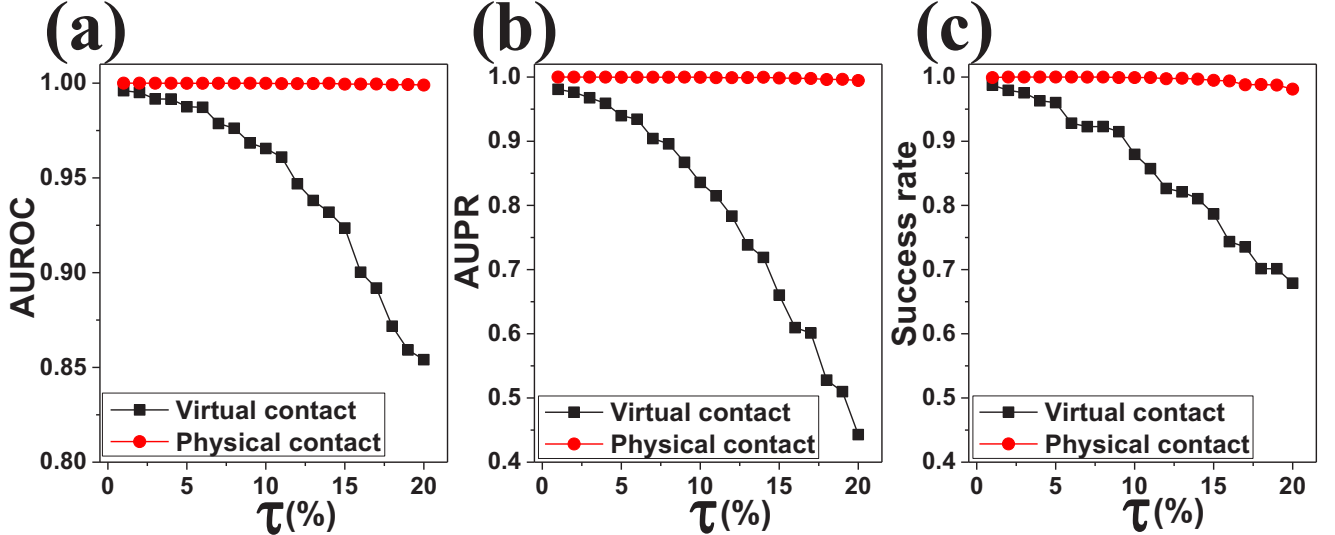


FIG. 9. **Impact of noise on reconstruction accuracy.** (a-c) AUROC, AUPR and Success rate versus the fraction  $\tau$  of randomly flipped states for a cyberphysical network with the ER-ER double-layer structure. The network parameters are  $N=100$ ,  $\langle k_1 \rangle = 4$ , and  $\langle k_2 \rangle = 6$ . The length of the time series is  $M=30000$ . Other parameters are the same as those in Fig. 3 in the main text.

- [37] C. Granell, S. Gómez, and A. Arenas, Phys. Rev. Lett. **111**, 128701 (2013).
- [38] Supporting Information contains details of the mathematical derivation of the reconstruction framework, additional numerical tests, and the effects of physical factors such as interlayer coupling, heterogeneous dynamical parameters, and noise on the reconstruction accuracy.
- [39] M. Magnani, B. Micenkova, and L. Rossi, arXiv preprint arXiv:1303.4986 (2013).
- [40] C. Ma, H.-F. Zhang, and Y.-C. Lai, Phys. Rev. E **96**, 022320 (2017).
- [41] J. Coleman, E. Katz, and H. Menzel, Sociometry **20**, 253 (1957).
- [42] J.-W. Li, Z.-S. Shen, W.-X. Wang, C. Grebogi, and Y.-C. Lai, Phys. Rev. E **95**, 032303 (2017).
- [43] D. J. Watts and S. H. Strogatz, Nature **393**, 440 (1998).
- [44] P. Erdos and A. Rényi, Publ. Math. Inst. Hung. Acad. Sci **5**, 17 (1960).
- [45] A.-L. Barabási and R. Albert, Science **286**, 509 (1999).